Features Extraction and Fuzzy Logic based Classification for False Positives Reduction in Mammographic Images

Arianna Mencattini, Giulia Rabottino, Marcello Salmeri, Roberto Lojacono and Eleonora Tamilia

University of Rome Tor Vergata, Dept. of Electronic Engineering
Via del Politecnico 1, 00133 Rome, Italy

Abstract. Breast cancer is one of the most common neoplasms in women and it is a leading cause of death worldwide. A proper screening procedure can help an early diagnosis of the tumor so reducing the death risk. A suitable computer aided detection system can help the radiologist to detect many subtle signs, normally missed during the screening phase, submitting to the radiologist's attention those regions that could contain an abnormality. However, one of the most critical problem deals with a suitable tradeoff regarding the number of suspicious zones to present to the radiologist and the capability of identifying the correct ones.
In this work, the classification of suspicious signs into normal tissue or massive lesions has been faced in order to get a False Positive Reduction without noticeably affecting the number of True Positives.

1 Introduction

Breast cancer is one of the most devastating causes of death among women in the world and mammography is still the most commonly used method for detecting breast cancer at early stages. However, radiologists can miss a significant portion of abnormalities. Some studies indicate that Computer Aided Detection systems (CADe) can provide a second opinion to the radiologists and potentially decrease the missed detection rate [1].

A CADe system used in breast cancer screening programs is composed by two main steps: the identification of suspicious regions and the false positives reduction [2] (see Fig. 1). Algorithms for the False Positive Reduction (FPR) of suspicious signs of disease, can work either with one view or with multiple views [3]. Tipically, the one-view FPR is a two classes classification task in which each Region Of Interest (ROI) can be classified as a mass or as normal breast tissue. A set of geometric and/or textural features have to be extracted and selected to train the classifier. Alternatively, *template matching* approaches can be used, comparing each extracted ROI with all the ROIs of a certain database using similarity measures or features vectors.

In this paper, we propose an FPR procedure based on the extraction of many different geometrical and textural features, their selection, and the classification of detected ROIs into normal or abnormal ones through a rule-based fuzzy inference system.

Mencattini A., Rabottino G., Salmeri M., Lojacono R. and Tamilia E..
Features Extraction and Fuzzy Logic based Classification for False Positives Reduction in Mammographic Images.
DOI: 10.5220/0003303500130025
In *Proceedings of the 2nd International Workshop on Medical Image Analysis and Description for Diagnosis Systems* (MIAD-2011), pages 13-25
ISBN: 978-989-8425-38-6
Copyright © 2011 SCITEPRESS (Science and Technology Publications, Lda.)

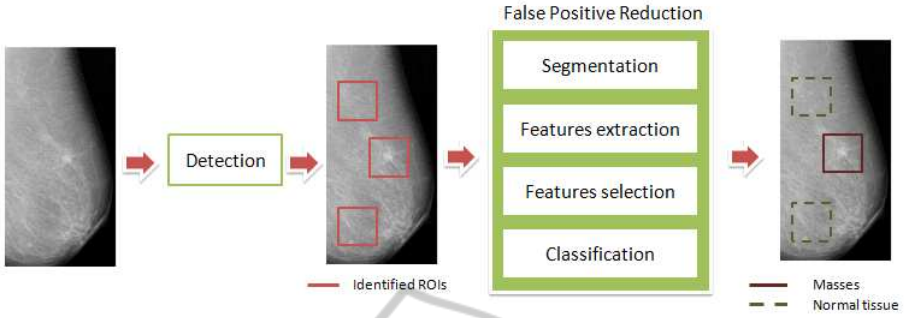

Fig. 1. CADe block scheme.

According to BIRADs lexicon [4] there are four different signs of breast disease in mammograms: masses, architectural distortion, calcifications, focal asymmetry.

- Masses are space occupying lesions seen in two different projections. They can have: *circumscribed margins* well-defined or sharply-defined; *indistinct margins* ill defined; *spiculated margins*, when the the lesion is characterized by lines radiating from the margins of the mass.
- Architectural distortion appear when the normal architecture is distorted with no definite mass visible. This includes spiculations radiating from a point, and focal retraction or distortion at the edge of the parenchyma. Architectural distortion can also be an associated finding.
- Focal asymmetry is a density that cannot be accurately described using the other shapes. It is visible as asymmetry of tissue density with similar shape on two views, but completely lacking borders and the conspicuity of a true mass. Additional imaging may reveal a true mass or significant architectural distortion.
- Calcifications are tiny deposits of calcium in the breast. Malignant calcifications are classified into: *amorphous or indistinct* calcifications often round or “flake” shaped calcifications; *coarse, heterogeneous* calcifications, irregular calcifications with varying sizes and shapes; *fine, pleomorphic or branching* calcifications, more conspicuous than the amorphous forms, varying in sizes and shapes. Benign calcifications are usually larger than calcifications associated with malignancy, coarser, often round with smooth margins and much more easily seen.

In particular, this study is devoted to the automatic massive lesions identification by CADe systems.

2 Methods for the Performance Evaluation

All the images used in this study belong to the Digital Database for Screening Mammography (DDSM) [5]. It contains 2275 studies, with two Cranio-Caudal (CC) views and two Medio-Lateral Oblique (MLO) views of each breast. The digital database has been obtained by digitalizing screen film mammographic images using four different scanners devices at three different hospitals in South Florida, with a spatial resolution

SCITEPRESS
SCIENCE AND TECHNOLOGY PUBLICATIONS

in the range $[42 - 50]$ μm and pixel resolution in the range $[12 - 16]$ bpp. Although the greatest request of the scientific community is at the moment to consider Direct Digital Databases, DDSM is the widest public mammographic images database available, with the most relevant variety of cases, including masses, calcifications and architectural distortions. Each study contains radiologist's report of the identified lesions, if present, including lesion type, position, biopsy proven assessment, boundary, subtlety, etc., according to BIRADs lexicon third edition. Radiologist's report can be used as the *ground-truth* for the detection procedure, while it would not be enough for the diagnosis step, since for example, margins of masses are not drawn accurately. Having the ground-truth, we can classify each ROI identified by the algorithm as a True Positive (TP), a False Positive (FP), or a True Negative (TN) and compute the *sensitivity* of the CADe and the number of False Positives per Image (FPpI). This task is recommended to compare our algorithm to the others proposed in the literature.

3 Mass Identification

In the first step, a CADe system extracts, from the original mammogram, suspicious regions on which the radiologists have to focus their attention. The method adopted for the automatic identification of masses in the mammographic images, analyzes the orientation of the gradient vectors in the image using circular support regions, to find highly compact structures with a growing luminance towards their center. The steps of this procedure are fully described in [6]. Here below, we only recall the basic ideas.

- *Decimate the original image.* Given the very large size of mammographic images in DDSM, we reduce resolution to the range $[400 - 500]$ μm. In this way, the algorithm can still identify the smallest masses with a diameter of 3 mm, but allows a fast computation.
- *Segment the background.* We isolate the breast region by implementing an active contour procedure and histogram thresholding in order to avoid the automatic identification be applied to the film background regions.
- *Grid the image.* Applying the algorithm only on a 5-pixels step grid.
- *Consider a circle with radius R around every point (i, j) of the grid* and compute on uniformly distributed $N = 24$ points on the circle (i.e., every 15 degrees) the following quantity:

$$x_R(i,j) = \frac{1}{N} \sum_{k,l \epsilon R} \cos\theta(k,l),$$

  where $\theta(k, l)$ is the angle between a gradient vector in (k, l) and the straight line connecting the pixels at (i, j) and (k, l) (see Fig. 2 left). The term $\cos\theta(k, l)$ represents a measure of the convergence of gradient vectors in the circle to the pixel of interest (i, j). When $x_R(i, j) = 1$ all the gradient vectors from the circle are oriented toward the same point. This occurs when the iso-intensity lines are concentric. It occurs when the pixel (i, j) is near the center of a massive lesion as one can see in Fig. 3. Figure 4 shows gradient vectors (blue lines) at every 5 pixels and iso-intensity lines (red lines) superimposed to a ROI containing a mass and to a ROI containing only normal tissue.

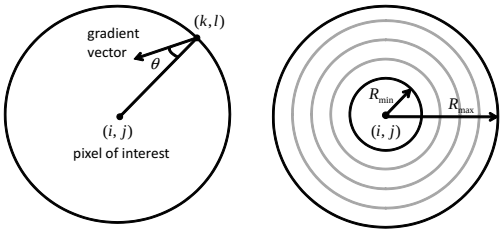

Fig. 2. Definition of the quantities (left) and iteration for different radii (right).

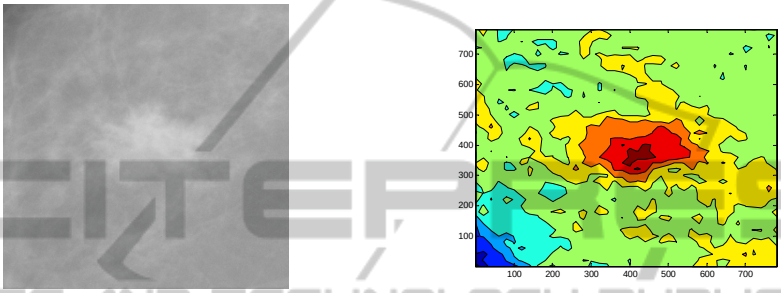

Fig. 3. A ROI containing a massive lesion (left) and the iso-intensity lines of the same ROI (right).

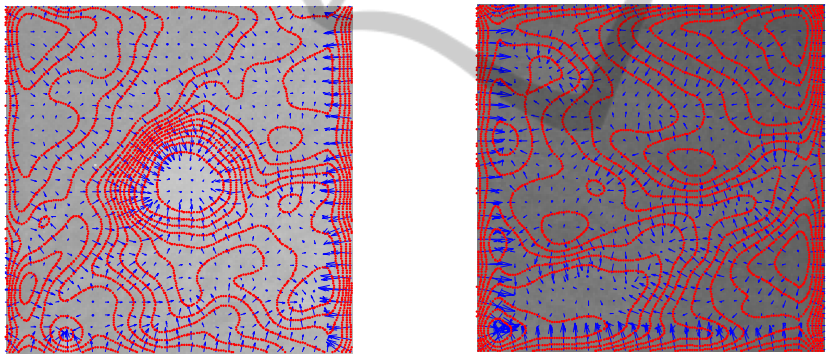

Fig. 4. Two ROIs containing a mass (left) and not a mass (right) with isointensity lines and gradient vectors superimposed.

– *Repeat for different radii* and compute, for every point (i, j) of the grid, the quantity:

$$x(i,j) = \underset{Rmin<R<Rmax}{mean} x_R(i,j).$$

Because masses have different diameters, from 3 to 40 mm, the region of support has to be adapted to all the possible sizes of the masses. In particular, we know that the radius of typical masses is in the range $[1.5 - 20]$ mm that for the considered not decimated image corresponds to $[30 - 400]$ pixels.

– *Sort the results.* In a preliminary phase, we show to the radiologist more than one option. All pixels (i, j) which exceed a certain percentage p of the maximum value

SCITEPRESS
SCIENCE AND TECHNOLOGY PUBLICATIONS

of $x(i,j)$ are presented to the radiologist and labeled in an ascending order: the more suspicious structures have the bigger markers. So, we have to choose the parameter p so that $x(i,j) > p \cdot \hat{x}$ where $\hat{x}$ is the maximum value of x for every i,j. Figure 5 shows two examples of the algorithm results: in the first case, the algorithm finds only one mass that corresponds to the radiologist marker and in the other case it finds 3 masses and the correct result is the mass labeled as the first. In our study we use $p = 0.80$.

– *Optimize.* All the markers that fall into adjacent centers are grouped to have a more readable result.

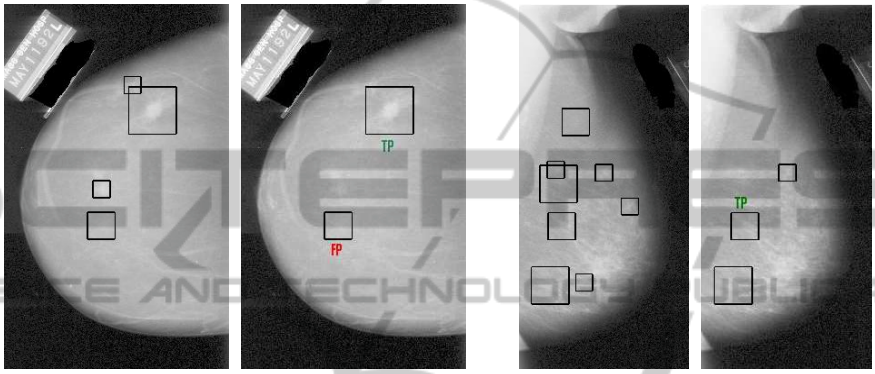

Fig. 5. Two examples of the algorithm output.

After the automatic identification step, we only consider images where true positives have been located by the algorithm, in order to separately assess the performance of the FPR step. So, we consider the better resulting cases, containing 157 ROIs with TPs and 312 ROIs with FPs. This setting provides an initial sensitivity equal to 1 and a mean FPpI equal to 2.2. The aim of our study is to reduce the number of FPpI, while preserving the sensitivity value the highest possible.

In order to introduce the reader to some of the problems encountered with the FPR step, we report in Fig. 6 some of the ROIs containing a false positive.

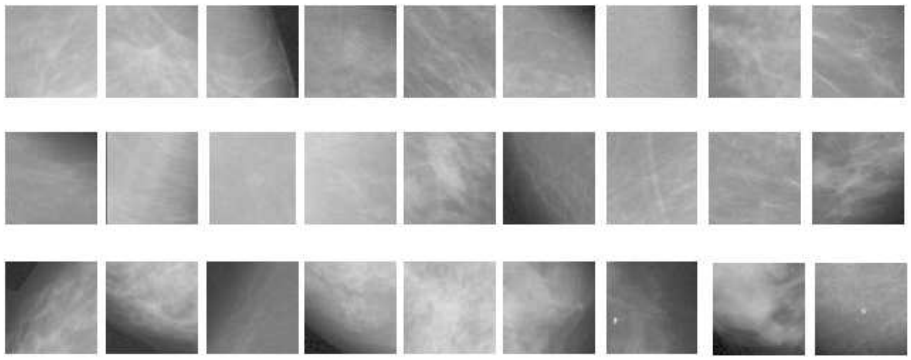

Fig. 6. Some examples of ROIs containing a false positive sign of disease.

4 Automatic Segmentation

After the identification algorithm locates suspicious signs in the mammogram, a ROI of fixed dimension is extracted around the identified point. In the following, the ROI is processed by a Fuzzy C-Means clustering algorithm to implement an intensity-based segmentation with a number of intensity levels equal to 5. The reconstructed image is then binarized considering as "foreground" only the largest group of adjacent pixels belonging to the cluster with the highest luminance level, and as "background" the remaining ones. Figure 7 shows some examples of the segmentation results for ROIs containing a mass and ROIs with false positives.

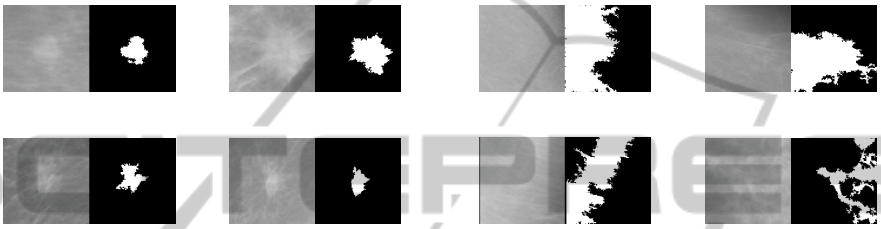

Fig. 7. Segmented ROIs containing a mass (left) and not a mass (right).

SCITEPRESS
SCIENCE AND TECHNOLOGY PUBLICATIONS

5 Features Extraction

The approach used in this work consists in testing a large set of features and then applying an automatic features selection algorithm in order to define a proper set of features with respect to a given training set. After the segmentation of the mass boundary, we have extracted the following features:

- Morphological features including area, circularity, eccentricity, roughness of the contour, elongation;
- Law's texture features [7]. Law proposed a method for classifying each pixel in an image based upon measures of local texture energy. The texture energy features represent the amounts of variation within a sliding window applied to several filtered versions of the given image. These measures are computed by first applying small convolution kernels to the image, and then performing a nonlinear windowing operation. The 2-D convolution kernels typically used for texture discrimination are generated from the following set of one-dimensional convolution kernels of length 5: $L5 = [1, 4, 6, 4, 1]$, $E5 = [-1, -2, 0, 2, 1]$, $S5 = [-1, 0, 2, 0, -1]$, $R5 = [1, -4, 6, -4, 1]$, $W5 = [-1, 2, 0, -2, 1]$. The operators listed above perform the detection of the following types of features: $L5$ local average (or level), $E5$ edges, $S5$ spots, $R5$ ripples, $W5$ waves. By combining in a nonlinear manner the above filters, we obtain 14 Texture Energy Measures (TEM) images. The most representatives are reported in Fig. 8 for a ROI containing an oriented pattern and one with a mass. Finally, for each of the 14 images, the following parameters are evaluated: mean, variance, kurtosis, and skewness.

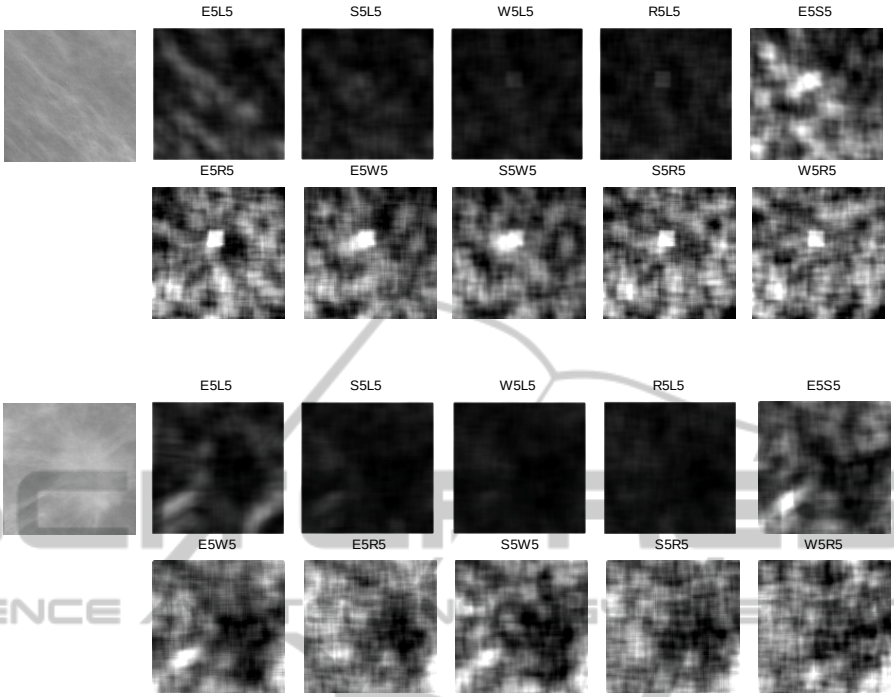

Fig. 8. Laws' texture energy measure for a ROI with a mass (bottom) and one with an oriented patter (up).

– Haralick texture features [8] are computed on the co-occurrence matrix extracted from the original ROI, from the ROI transformed by nonlinear contrast enhancement, from the ROIs transformed by the Ranklet Transform [9], and finally from the ROI elaborated by Sobel filters at different sizes. In particular, the ranklet transform is an orientation-selective, non-parametric and multi-resolution transform which has already been successfully exploited in image classification tasks, specifically face recognition in image frames [10]. The ranklet transform of an image involves three phases: multiresolution, orientation-selective, and non-parametric analysis. Fig. 9 shows some examples of the same ROIs above processed by Ranklet transform, at three different resolution factors (4, 6, and 14).

6 Features Selection

At a preliminary step, more than 1000 features have been extracted and a ranking by a specific selection criterion has been applied on this set. Features have been evaluated one by one, in order to assign a score to each of them according to its relevance, evaluated on a training set.

Three indexes have been computed in this study, leading to different *working points* (i.e., different possible trades off among the ability of reducing false positives, while preserving true positives):

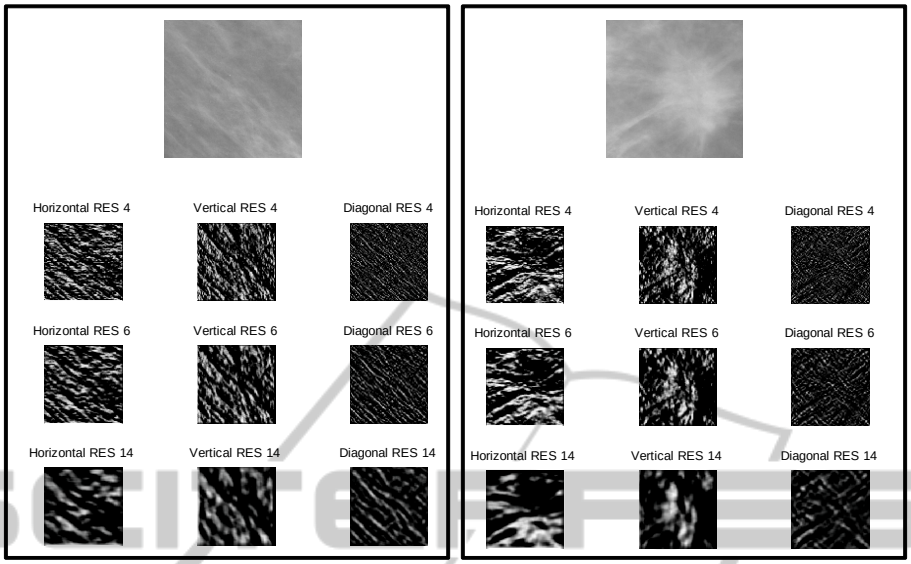

Fig. 9. Ranklet transform at three different resolutions of a ROI with a mass (bottom) and one with an oriented pattern (up).

SCITEPRESS
SCIENCE AND TECHNOLOGY PUBLICATIONS

– the difference between the rate of ROIs correctly recognized as normal tissue in the initial amount of false positives and the rate of wrongly recognized ROIs as normal tissue in the initial amount of true positives:

$$IND_1 = \frac{TN}{TN+FP} - \frac{FN}{TP+FN};$$

– the difference between the improvement of the correctness and the decrease of the sensitivity:

$$IND_2 = \left[\frac{TP}{TP+FP} - \frac{sTP}{sTP+sFP}\right] + \left[\frac{TP}{TP+FN} - 1\right];$$

– how much the false positive reduction is stronger than the loss of false positives, leading to an increasing of false negative ROIs:

$$IND_3 = 1 - \frac{FN}{TN};$$

Using the cited indexes, we denote the three different ranking vectors as RKC_1, RKC_2, and RKC_3.

As last step, it was necessary to find out the optimal number of features among those ranked. Actually, the performance of the system can not be uniquely assessed, because they depend on the radiologist's needs and expectation. The radiologist, in fact, could require the CADe system providing the minimum number of False Positives per mammogram, that is the maximum reduction of the number of *FPpI* even in spite of a

reduction of *sensitivity*, in order to avoid too much false suggestions which could divert away attention from the real mass. Otherwise, the radiologist may not require first of all any losses of *sensitivity*, even at the expense of a low reduction of false positives. In this case, the radiologist prefers receiving even many suggestions but always including the real mass, when it is present. Section 8 will provide some numerical examples for these options.

7 Fuzzy Classification

A Fuzzy Inference System (FIS) has been implemented and used for the classification of ROIs into abnormal or normal breast tissue [11]. To decide an appropriate diagnosis in one patient, we introduce three non-fuzzy sets, as explained in [11].

- The set of symptoms (corresponding to the set of features) $S = \{S_1, S_2, ..., S_n\}$.
- The set of diagnosis $D = \{D_1, D_2, ..., D_p\}$ (where, in this case, $p = 2$ because of the presence of two classes, "Cancer (C)" or "Normal (N)" that is ROI containing a mass or ROI containing normal tissue).
- The set of patients $P = \{P_1\}$ (the set of ROIs cropped from the mammograms of a patient).

SCITEPRESS
SCIENCE AND TECHNOLOGY PUBLICATIONS

The assignment of a diagnosis to the patient requires the evaluation of two distinct relations: the *Patient-Symptom Relation* (PS) where the different symptoms are evaluated in the mammograms of the considered patient; the *Symptom-Diagnosis Relation* (SD) where the importance of each symptom for the diagnosis (C or N) is evaluated. This procedure is at a preliminary investigation stage, and at present it computes simply the positive predictive value and the negative predictive values of each feature independently, for each patient in the training set, leading to the so called incidence level of the symptom to the diagnosis. Hence, the symptoms occurring in a set S are associated with the diagnosis from set D (SD) and further they are associated in turn with the patient P (assuming that information about all symptoms in S is complete in the patient's case), in order to establish the final *Patient-Diagnosis Relation* (PD).

7.1 Fuzzy Inference Engine

A necessary step for the implementation of a FIS is the definition of a set of fuzzy rules which relate the input values (the symptoms) to the output values (the diagnoses). The fuzzy rules are defined according to the two above described *relations* and clinical experience, according to [11]. In particular the following rules

$$\begin{aligned} if \quad & \underbrace{(symptom\, S_j \ is\ a\, decisive\, feature\, for\ diagnosis\, B)}_{SD\, relation} \\ and \quad & \underbrace{(symptom\, S_j \ is\ present\ in\ patient\, P)}_{PS\, relation} \\ then \quad & \underbrace{(diagnosis\, B \ is\ assigned\, to patient\, P)}_{PD\, relation} \end{aligned}$$

are defined, which consider only one symptom at a time. In general, for each symptom, 4 rules could be written which combine *N* and *M* diagnoses and *low* and *high* presence of the symptom in the patient. However, the experience and the data lead to conclude that, for a certain symptom S_j, *low* means presence of mass and *high* means normal tissue, or vice versa. Hence, only a subset of possible rules are implemented. In the considered application, the output values are crisp (either N or M). This means that the considered FIS is simplified with respect to the general case where also the output variables are fuzzy sets. Hence, the defuzzification step is not required and, in order to associate the final membership degrees to the two final diagnoses (N, M), the following quantities can be considered [11]:

$$\mu_N = \frac{\sum_{j=1}^{N_{opt}} IL(S_j^N) \cdot \mu_{l/h}(S_j)}{\sum_{j=1}^{N_{opt}} IL(S_j^N)} \quad \mu_M = \frac{\sum_{j=1}^{N_{opt}} IL(S_j^M) \cdot \mu_{l/h}(S_j)}{\sum_{j=1}^{N_{opt}} IL(S_j^M)}$$

where N_{opt} is the selected optimal number of features ranked according to one of the three criterions shown above, and $IL(S_j^{N/M})$ denotes the incidence of feature S_j to the diagnosis N/M. μ_N provides the degree of *not abnormality* of the considered ROI, while μ_M provides the degree of abnormality of the same ROI. So, the outputs of the fuzzy inference system are: the *credibility degree* that the ROI is a mass (μ_M) and the *credibility degree* that the same ROI is normal breast tissue (μ_N). Differently from standard classifiers, these two indexes are not complementary to the unity. These values have to be compared to provide the final decision.

SCITEPRESS
SCIENCE AND TECHNOLOGY PUBLICATIONS

8 Results

For the performance evaluation of the fuzzy classifier, a *leave-one-out* cross-validation technique has been adopted: the training set was composed of the entire dataset of ROIs except one which is used as test. This procedure is repeated for each features vector in the training set. The optimal number of features to be used is different according to the ranking and to the selection criterion. In particular, using the same criterion for both ranking and selection of the optimal number, we obtain $NP_{opt} = 90$ for criterion IND_1, $NP_{opt} = 39$ for criterion IND_2, and $NP_{opt} = 27$ for criterion IND_3. The results of the classification using the three methods are reported in Table 1, in the columns identified with *No Threshold*. It means that the final decision is taken only by comparing credibility degrees of abnormality and of not abnormality.

8.1 Uncertain Diagnosis: *Certainty Threshold*

The reported results exhibit a $sensitivity$ always greater than 0.8 and a $correctness$ increased from 0.33 up to 0.5-0.7, with a number of FPpI that varies according to the used criterion in the range $[0.3 - 0.97]$. Moreover, another important aspect has to be considered. The fuzzy logic classifier assigns to each ROI under analysis two values thus not conferring a single judgment of membership to a class. These membership degrees have to be compared to make a decision, but this comparison can not be sufficient. It is important to analyze the difference between μ_M and μ_N in order to take

into account the natural variability of these degrees. Hence a *certainty threshold* has been empirically set to 0.15. This threshold has been set low enough in order to exclude just the most evident doubtful cases. If the absolute value of $(\mu_M - \mu_N)$ was less than 0.15, a conservative choice is to classify the ROI as abnormal. Thus, every doubtful case can be further analyzed by the radiologist or by the computerized system. Table 1 shows the results obtained adopting this modified approach, in the columns identified by *Threshold*. Using this threshold, the number of positives increases, thus causing the

Table 1. Results of classification with a *certainty threshold* equal to 0.15, compared with the previous results without any threshold.

	IND_1		IND_2		IND_3	
	Threshold	No Threshold	**Threshold**	No Threshold	**Threshold**	No Threshold
TP	147	126	157	153	157	156
FN	10	31	0	4	0	1
TN	210	264	183	198	105	159
FP	102	48	129	114	207	153
SENS	**0.9363**	0.8025	**1**	0.9745	**1**	0.9936
FPpI	**0.65**	0.30	**0.82**	0.72	**1.31**	0.97

SCITEPRESS
SCIENCE AND TECHNOLOGY PUBLICATIONS

increase in both True Positives and False Positives with respect to the *No Threshold case*. At the same time, the working point shifts toward a greater sensitivity, with an acceptable increase in $FPpI$. All these results prove that the features ranking/selection algorithms, the fuzzy classifier, and the conservative setting achieved by the certainty threshold perform well and can be easily adapted to different requirements of the radiologists assigning to the CADe a good flexibility and adaptability to different clinical scenarios.

9 Comparisons

We report also the most relevant results described in the literature concerning the False Positive Reduction in the automatic detection of breast masses. In particular, Li et al. [12] used a soft neural network decision classification. Angelini et al. [13] proposed a support vector regression filtering approach. Masotti et al. [9] reduced false positives via gray scale invariant ranklet texture features using a support vector machine classifier for discrimination. Tourassi et al. [14] used a template matching scheme based on mutual information. Varela et al. [15] employed a neural network classifier to merge different combination of features. All the results are compared in Table 2 in terms of the True Positive Reduction (TPR) and the False Positive Reduction (FPR). The number of ROIs used in the studies is also reported. We also insert our results obtained by criterion IND_2.

10 Conclusions

In this work, we presented a study on the False Positives Reduction in the automatic breast masses identification in mammographic images. We addressed the FPR step as

Table 2. Comparisons of different methods for false positive reduction.

	TPR	FPR	ROIs
Li et al.	1%	56%	25
Angelini et al.	13%	38%	69
Tourassi et al.	10%	65%	1820
Varela et al.	22%	85%	120
Masotti et al.	0%	30%	884
Proposed method	**0%**	**58%**	**469**

a two classes classification problem, with the aim to assign to each suspicious ROI a degree of abnormality and a degree of not abnormality, thus reducing the whole number of ROIs to be presented to the radiologist. A large set of features have been extracted from the ROIs identified by an automatic identification algorithm proposed by the authors. Then, the selected features have been used to train a fuzzy classifier, properly structured for medical applications. Different working points have been considered so that the radiologist could choose the best tradeoff between sensitivity and false positive per image, according to the clinical application.

SCITEPRESS
SCIENCE AND TECHNOLOGY PUBLICATIONS

References

1. M. Bazzocchi and F. Mazzarella, "CAD systems for mammography: a real opportunity? A review of the literature," http://www.springerlink.com/content/x3157r8u72196h45/ fulltext.pdf/, 2006.
2. A. Oliver, "A new approach to the classification of mammographic masses and normal breast tissue," in Proceedings of the 18th International Conference on Pattern Recognition, 2006, vol. 4, pp. 707 – 710.
3. J. Wei, H-P. Chan, B. Sahiner, C. Zhou, and L. M. Hadjiiski, "Computer-aided detection of breast masses on mammograms: Dual system approach with two-view analysis," Med. Phys., vol. 36, no. 10, pp. 4451 – 4460, 2009.
4. C. Balleyguier, S. Ayadi, K. Van Nguyen, D. Vanel, C. Dromain, and R. Sigal, "BIRADS classification in mammography," European Journal of Radiology, vol. 61, pp. 192–194, 2007.
5. University of South Florida, "DDSM: Digital database for screening mammography," http://marathon.csee.usf.edu/Mammography/Database.html, 2000.
6. A. Mencattini, G. Rabottino, M. Salmeri, and R. Lojacono, "Assessment of a breast masses identification procedure using an iris detector," IEEE Transactions on Instrumentation and Measurement, in press.
7. K. I. Laws, "Laws' texture measures," http://www.ccs3.lanl.gov/ kelly/ZTRANSITION/ notebook/laws.shtml, 2001.
8. R. M. Haralick, "Statistical and structural approaches to texture," Proceedings of the IEEE, vol. 67, no. 5, pp. 786 – 804, 1979.
9. M. Masotti, N. Lanconelli, and R. Campanini, "Computer aided mass detection in mammography: False positive reduction via gray scale invariant ranklet texture features," Medical Physics, vol. 36, no. 2, 2009.
10. F. Smeraldi, "Ranklets: Orientation selective non-parametric features applied to face detection," in 16th International Conference on Pattern Recognition, 2002, vol. 3, pp. 351 – 359.

11. E. Rakus-Andersson, Fuzzy and rough techniques in Medical Diagnosis and Medication, Springer-Verlag, 2007.
12. L. Li, Y. Zheng, L. Zhang, and R. A. Clark, "False-positive reduction in cad mass detection using a competitive classification strategy," Medical Physics, vol. 28, 2001.
13. E. Angelini, R. Campanini, and A. Riccardi, "Support vector regression filtering for reduction of false positives in a mass detection cad scheme: Preliminary results," http://amsacta.cib.unibo.it/archive/00000912/01/angelini05support.pdf, 2005.
14. G. D. Tourassi, R. Vargas-Vorecek, D. M. Catarious, and C. E. Floyd, "Computer assisted detection of mammographic masses: a template matching scheme based on mutual information," Medical Physics, vol. 30, no. 8, pp. 2123 – 2130, 2003.
15. C. Varela, P. G. Tahoces, A. J. Mendez, M. Souto, and J. J. Vidal, "Computerized detection of breast masses in mammograms," Computers in Biology and Medicine, vol. 37, pp. 214 – 226, 2007.

SCITEPRESS
SCIENCE AND TECHNOLOGY PUBLICATIONS